JAERI-M
9179

ACCUMULATION AND ELIMINATION OF METAL IMPURITIES NEAR THE CENTER OF DEE PLASMAS IN DOUBLET III

(Doublet-III Experimental Report, 3)

November 1980

N. FUJISAWA, S. KONOSHIMA, M, NAGAMI, S. SEKI
H. YOKOMIZO, M. SHIMADA, G. L. JAHNS,* S. EJIMA,*
R. GROEBNER,* N. H. BROOKS,* and A. KITSUNEZAKI

日本原子力研究所
Japan Atomic Energy Research Institute

Accumulation and Elimination of Metal Impurities near the Center of Dee Plasmas in Doublet III
(Doublet III Experimental Report, 3)

Noboru FUJISAWA, Shigeru KONOSHIMA, Masayuki NAGAMI,
Shogo SEKI, Hideaki YOKOMIZO, Michiya SHIMADA,
Gary L. JAHNS*, Seiki EJIMA*, Richard GROEBNER*,
Neil H. BROOKS*, and Akio KITSUNEZAKI
Division of Large Tokamak Development,
Tokai Research Establishment, JAERI
(Received October 16, 1980)

Impurity accumulations are observed near the center of the dee-shaped plasma in Doublet III. The accumulation causes remarkable changes in the current profile. This tendency to accumulate is counteracted by MHD activities.

Keywords : Doublet III tokamak, Impurity, Accumulation, Elimination

---

* General Atomic Co., U.S.A.

This work was done under a cooperative agreement between the United States Department of Energy and the Japan Atomic Energy Research Institute
USDOE Contract No. DE-AT03-80ET51019

Doublet Ⅲ D型プラズマ中心近くの金属不純物の集中と放出
(ダブレットⅢ実験報告・3)

日本原子力研究所東海研究所大型トカマク開発部
藤沢　登・木島　滋・永見　正幸・関　省吾
横溝　英明・嶋田　道也・G. L. Jhans*・S. Ejima*
R. Groebner*・N. H. Brooks*・狐崎　晶雄

(1980年10月16日受理)

Doublet ⅢD型プラズマの中心近くで観測される不純物集中と放出について報告する。この集中現象はプラズマ電流の分布を顕著に変える。また，この集中現象はプラズマ中のMHD振動により消えてしまう。

* General Atomic Company, U.S.A

Contents

1. Introduction 1
2. Experiments 2
3. Effective Ionic Charge Profile 3
4. Discussion 4
5. Conclusion 7
Acknowledgment 8
References 8

目　　次

1. 序 1
2. 実験結果 2
3. 実効電荷数 3
4. 考　察 4
5. 結 7
謝　辞 8
参考文献 8

1. INTRODUCTION

It is well known that impurity contamination is a primary obstacle to obtaining reactor grade tokamak plasmas. In present-day tokamaks, light impurities can be successfully reduced by sufficient discharge cleaning (Ref. 1) and/or via titanium gettering (Ref. 2). Research on the mechanism of metal impurity release and the suppression of metal impurity influx has also progressed recently (Refs. 3, 4). Therefore, the behavior of the metal impurities in the plasma takes on greater importance. Of particular interest is whether impurities in large tokamaks accumulate near the plasma center (Ref. 5).

In the Doublet III device, plasmas with $Z_{eff} < 2$ have been obtained by sufficient discharge cleaning. In low density and high current discharges, appreciable metal impurity radiation is observed, characterized by nickel, a principal constituent of both walls and limiters. Moreover, mental impurities are observed to accumulate at the plasma center. This tendency to accumulate is counteracted suddenly by MHD activities which seem to enhance the transport near the plasma center, with metal impurities near the plasma center being pumped out.

In this paper, we describe the experimental results on the accumulation and elimination of metal impurities near the plasma center in dee-shaped discharges in Doublet III, and discuss the disappearance of the impurity accumulation.

2. EXPERIMENTS

The dee plasmas in the D-III device have an elliptical cross section. The main results are described elsewhere (Ref. 6). The elongation of the plasma cross section described here is around 1.2, and the major and minor radii are 1.43 m and 0.45 m, respectively. The vacuum chamber and the limiter are Inconel.

The time evolutions of discharge current, loop voltage, line-averaged electron density and the central value of the electron temperature are shown in Fig. 1. Assuming uniform effective ionic charge, $Z_{eff} \simeq 1.5$ is obtained at 0.6 s. The toroidal magnetic field is 20 kG, and the discharge current of 0.38 MA corresponds to a safety factor of 3.74 at the limiter.

The time behavior of soft X-ray detectors is shown in Fig. 2. The detectors look at the plasma tangentially on a midplane. The channel 3 detector sights the plasma center on the major radius at 1.43 m. The difference among the major radii which each detector sights is 3 cm. After a slightly unstable period in an initial stage, the soft X-ray signals near the center (ch 1 - 4) increase up to 0.3 s, and become steady. At 0.41 s, the soft X-ray signals near the center suddenly go down; however, the signals of channels 6 - 10 hardly change. During the period of the decrease in the soft X-ray signals, strong MHD oscillations are observed on channels 1 - 5.

The 95.85Å spectral line, characteristic of NiXXI, is measured by the VUV spectroscope and is also displayed in Fig. 2. The time behavior of the NiXXI is quite similar to those of the soft X-ray signals near the

center. Judging from the central electron temperature, the NiXXI is considered to be emitted near the plasma center. The large soft X-ray signals near the center are due to the nickel impurity. On the other hand, the NiXI as revealed through a spectral line at 140Å remains nearly constant during the steady state phase of a discharge; this can be interpreted to mean that the influx of nickel is constant. The metal impurity has a tendency to accumulate near the plasma center, and that tendency to accumulate is counteracted by the MHD oscillations observed on the signals in the soft X-ray there. After the decrease in the soft X-ray near the center, the sawtooth oscillations are observed on the soft X-ray signals. This fact indicates that the q value near the center is less than one.

3. EFFECTIVE IONIC CHARGE PROFILS

The microwave radiometer measurements of the electron temperature profiles before and after the onset of MHD oscillations are shown in Fig. 3. The temperature profile before the MHD oscillations is more peaked than the one after the oscillation. If the effective ionic charge Z_{eff} is uniform over the plasma cross-section, the sawtooth oscillation should appear before the MHD oscillation. However, as mentioned above, the experimental results indicate that the sawtooth oscillations are observed after the oscillations, never before. This fact suggests that the profile of Z_{eff} before the MHD oscillation is centrally peaked.

The profiles of the soft X-ray intensities before and after the MHD

oscillations are shown in Fig. 4. It is noted that the profile before the MHD activities is strongly peaked near the center, compared with the one after the MHD oscillations. The signals in channels 6 - 10 of the soft X-ray array seldom change before and after the oscillations.

The absolute values detected by the soft X-ray array can be compared with calculation based on bremsstrahlung and recombination process (Ref. 7). Using the electron temperature profiles presented in Fig. 3 and an assumed parabolic density profile, the calculated hydrogen bremsstrahlung for a Maxwellian plasma after the MHD oscillations is plotted as a dotted line in Fig. 4. As a matter of course, the enhancement of the signal above the hydrogenic value due to the presence of impurities (the so-called enhancement factor) has to be taken into account in order to adjust the calculated value to the experimental one.

The best fit to the data is shown in Fig. 4. The profiles of the enhancement factor used in the calculation are presented in Fig. 5. The enhancement factor before the MHD oscillations reveals a strong peaking. After the MHD activity, however, hollow profile of the enhancement factor is required to adjust the calculation to the data.

4. DISCUSSION

The effective ionic charge Z_{eff} can be calculated from the enhancement factor (Ref. 7). The obtained profiles of the Z_{eff} are shown in Fig. 5. In the derivation of Z_{eff} (r), the metal impurity is assumed to be iron. The observed main metal impurity is nickel, as above-mentioned. There is no available data on nickle, so data on iron is adopted, instead.

Since the difference between nickel and iron is considered to be small, the Z_{eff} values in the calculation on iron can be useful for nickel. The Z_{eff} values in the region outside the r = 30 cm surface cannot be determined because the bremsstrahlung from this region does not contribute to the signal; thus the Z_{eff} value can have a large error bar.

As mentioned previously, the Z_{eff} values after the MHD oscillation is around 1.5, assuming a uniform Z_{eff}. As shown in Fig. 5, the Z_{eff} value from the soft X-ray signals is almost 1.6. The derivation of the Z_{eff} from the soft X-ray signals is believed to be accurate.

The effective ionic charge Z_{eff} before the MHD oscillations has a strongly peaked profile near the plasma center. On the other hand, the profile after the MHD oscillation is slightly hollow. It is concluded that the metal impurity is accumulated in the plasma center before the oscillation, and the metal impurity is eliminated from the center with the MHD activities.

The current profile can be derived from the electron temperature, the effective ionic charge, and the electric field. The period which we are now discussing is long compared to characteristic times for the relevant physical processes, i.e., 0.1 s and 0.2 s before and after the oscillation, respectively. Therefore, it is a good assumption that the loop voltage is uniform over a plasma cross-section. The calculated results on the current distribution are shown in Fig. 6. In the calculation, it is assumed that Z_{eff} in the region of r > 30 cm is the same as that at r = 30 cm. The total discharge currents from the calculated results are 1.16 and 1.05 times as much as the observed discharge current of

380 kA. Such minor discrepancies can be accounted for by the soft X-ray sensitivity, the calculation of the emission from the plasma, and the derivation of the Z_{eff} values. Then, the calculated current distribution is normalized to the observed discharge current, and is shown in Fig. 6.

Figure 7 shows the profiles of the safety factor calculated from the current distribution in Fig. 6. The experimental data indicate that the electron temperature profile before the MHD oscillations is more peaked than the one after the oscillations, and that the sawtooth oscillations are observed after the MHD oscillations, never before the oscillations. The profiles shown in Fig. 7 successfully explain these puzzling phenomena. The impurity accumulation in the plasma center prevents the safety factor being less than one, and the impurity evacuation from the plasma center increases the current density in the center and helps to drive q (o) to less than one.

The metal impurity content near the plasma center is determined by the imbalance between the influx and the outflux of the impurity. The MHD oscillations seem to enhance the transport, and the metal impurity in the center decreases. However, the quantity of the metal impurity after the oscillation is more than 0.1%, a value that is comparable to the requirement for future larger machines. However, the impurity concentration prior to the onset of MHD activity exceeds 1%, which is a very severe condition. It is necessary to decrease the metal influx from the wall and to enhance the outflux of the impurity due to the enhanced transport. In discharges with higher densities, such impurity accumulation is not observed. This seems to be due to the reduction of

the impurity influx and to the enhanced transport induced by the MHD activity.

The reason why the plasma before the MHD oscillation suddenly becomes unstable is not clear. Plasmas with hollow current profiles seem to have a greater tendency to display such instabilities. This point must be studied further.

In this paper, the contribution of light impurities (e.g. oxygen) is excluded. Because there is no data on highly ionized light impurity ions (e.g. OVIII, OVII), there is no way to evaluate the effect of light impurities. But, it is reasonable that light impurities contribute to Z_{eff} to some extend. The almost similar conclusions (current profile) can be drawn. Qualitative spectroscopic study should be made infuture.

5. CONCLUSION

The peaked profile in the soft X-ray signals observed in relatively low density discharges is seemed to be due to the metal impurity accumulation near the plasma center. The major metal impurity is nickel from the limiter and the vacuum wall. During the stage in which impurities accumulate, the profile of the discharge current becomes hollow. The impurity accumulation is suddenly counteracted by MHD activities, which may be a consequence of the hollow current profile. The MHD activities enhance the impurity transport, and eject metal impurities from the plasma center. This leads to a slightly hollow profile of Z_{eff}. The safety factor corresponding to the deduced current profile is less than one near the center, which is in agreement with the observed sawtooth oscillations.

Acknowledgment

We are grateful to Dr. T. Ohkawa and the Doublet III staff members of the General Atomic Company for their assistance in the experiment. Drs. S. Mori, Y. Iso, Y. Obata and M. Yoshikawa of JAERI are gratefully acknowledged for their continuous encouragement of our work.

References

1. L. Oren and R. J. Taylor, Nucl. Fusion 17 (1977) 1143.
2. P. E. Stott, C. C. Daughney, and E. A. Ellis, Nucl. Fusion 15 (1975) 431.
3. K. Ohasa, S. Sengoku, H. Maeda, H. Ohtsuka, S. Yamamoto, S. Kasai, M. Nagami, K. Odajima, H. Kimura, and Y. Shimomura, J. Phys. Soc. Japan 46 (1979) 1635.
4. N. Suzuki, N. Fujisawa, S. Konoshima, M. Maeno, M. Shimada, T. Yamamoto, S. Kasai, and K. Uehara, in Controlled Fusion and Plasma Physics (Proc. 9th Europ. Conf. Oxford, 1979) Vol. 1 (1979).
5. J. B. Taylor, Nucl. Fusion Special Supplement 1974, IAEA, Vienna (1974) 403.
6. A. Kitsunezaki, S. Konoshima, M. Nagami, S. Seki, M. Shimada, and H. Yokomizo, and D-III Group, Bull. APS 24 (1979) 1096.
7. S. von Goeler, W. Stodiek, H. Eubank, H. Fishman, S. Grebenshchikov, and E. Hinov, Nucl. Fusion 15 (1975) 301.

Figure Captions

Fig. 1 Time behavior of loop voltage (V_L), discharge current (I_p), mean electron density ($\bar{n}_e$), and central electron temperature of dee hydrogen plasmas in D-III.

Fig. 2 Time evolution of array of soft X-ray detectors (10 channels) and NiXXI (95.85Å). The soft X-ray detectors sight a plasma tangentially on a midplane. Arrows before and after MHD oscillations show the time analyzed in this report.

Fig. 3 Radial profiles of electron temperature measured with microwave radiometer of the second harmonic of the electron cyclotron frequency before and after MHD activity.

Fig. 4 Profiles of soft X-ray intensity. Marks (O) and (Δ) are observed data before and after MHD activities, respectively. The solid and broken lines are the best fits obtained using the enhancement factors in Fig. 5. The dotted line is hydrogen bremsstrahlung after MHD oscillations assuming a parabolic density profile and using the temperature profile in Fig. 3.

Fig. 5 Radial profiles enhancement factors ζ^b before, and ζ^a after MHD activities giving best fits are shown in Fig. 4. Profiles of effective ionic charge (Z_{eff}) derived from enhancement factors, assuming that the main impurity is iron.

Fig. 6 Radial profiles of discharge current density before and after MHD oscillations calculated from loop voltages, temperature profiles, and effective ionic charge profiles.

Fig. 7 Profiles of safety factors calculated from profiles of current densities in Fig. 6.

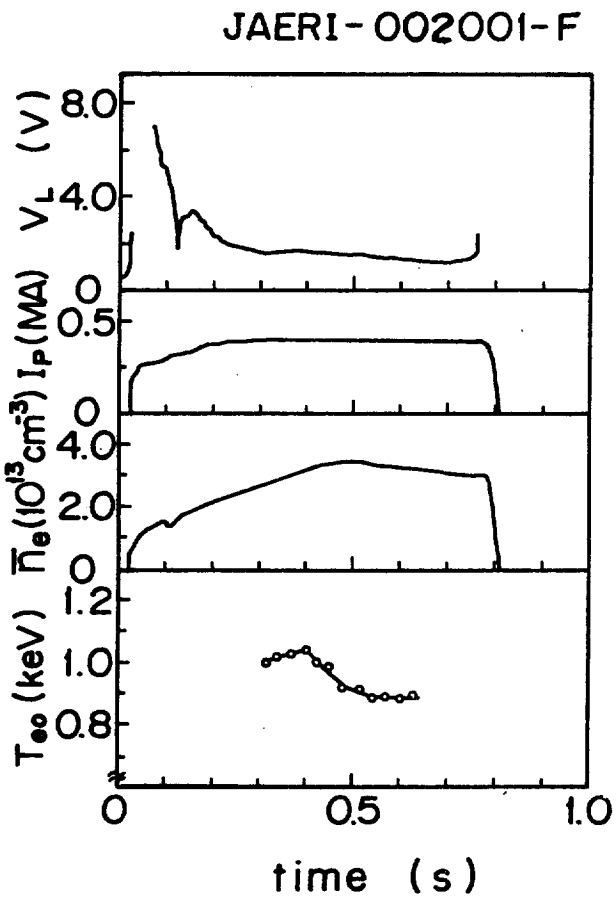

Fig. 1

Time behavior of loop voltage (V_L), discharge current (I_p), mean electron density ($\bar{n}_e$), and central electron temperature of dee hydrogen plasmas in D-III.

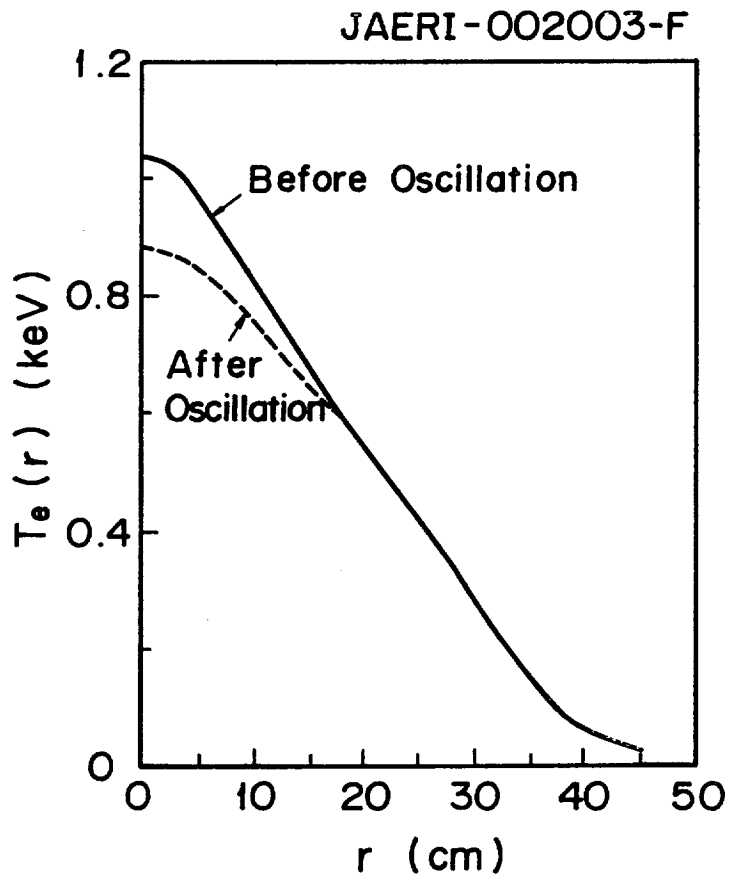

Fig. 3

Radial profiles of electron temperature measured with microwave radiometer of the second harmonic of the electron cyclotron frequency before and after MHD activity.

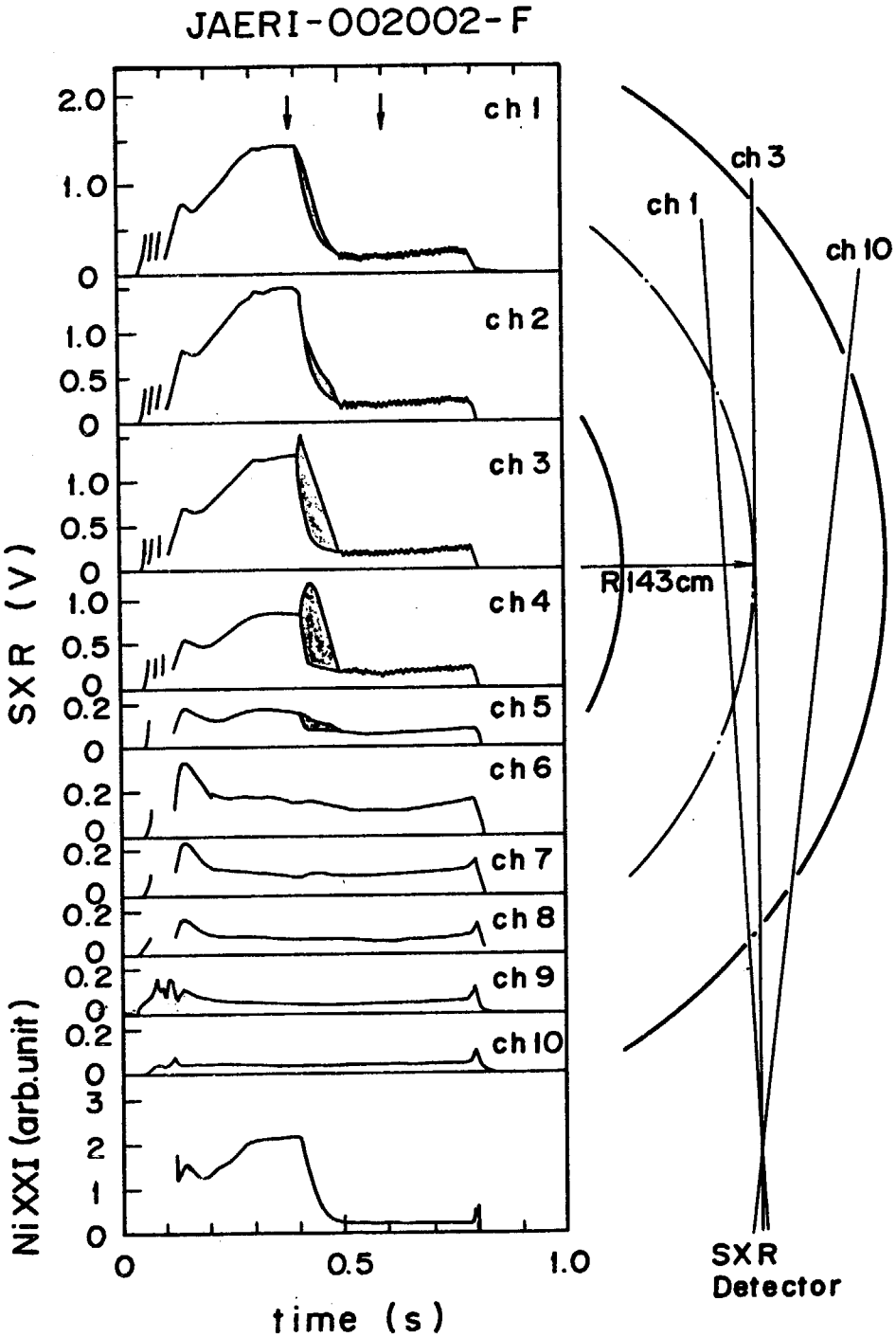

Fig. 2 Time evolution of array of soft X-ray detectors (10 channels) and NiXXI (95.85Å). The soft X-ray detectors sight a plasma tangentially on a midplane. Arrows before and after MHD oscillations show the time analyzed in this report.

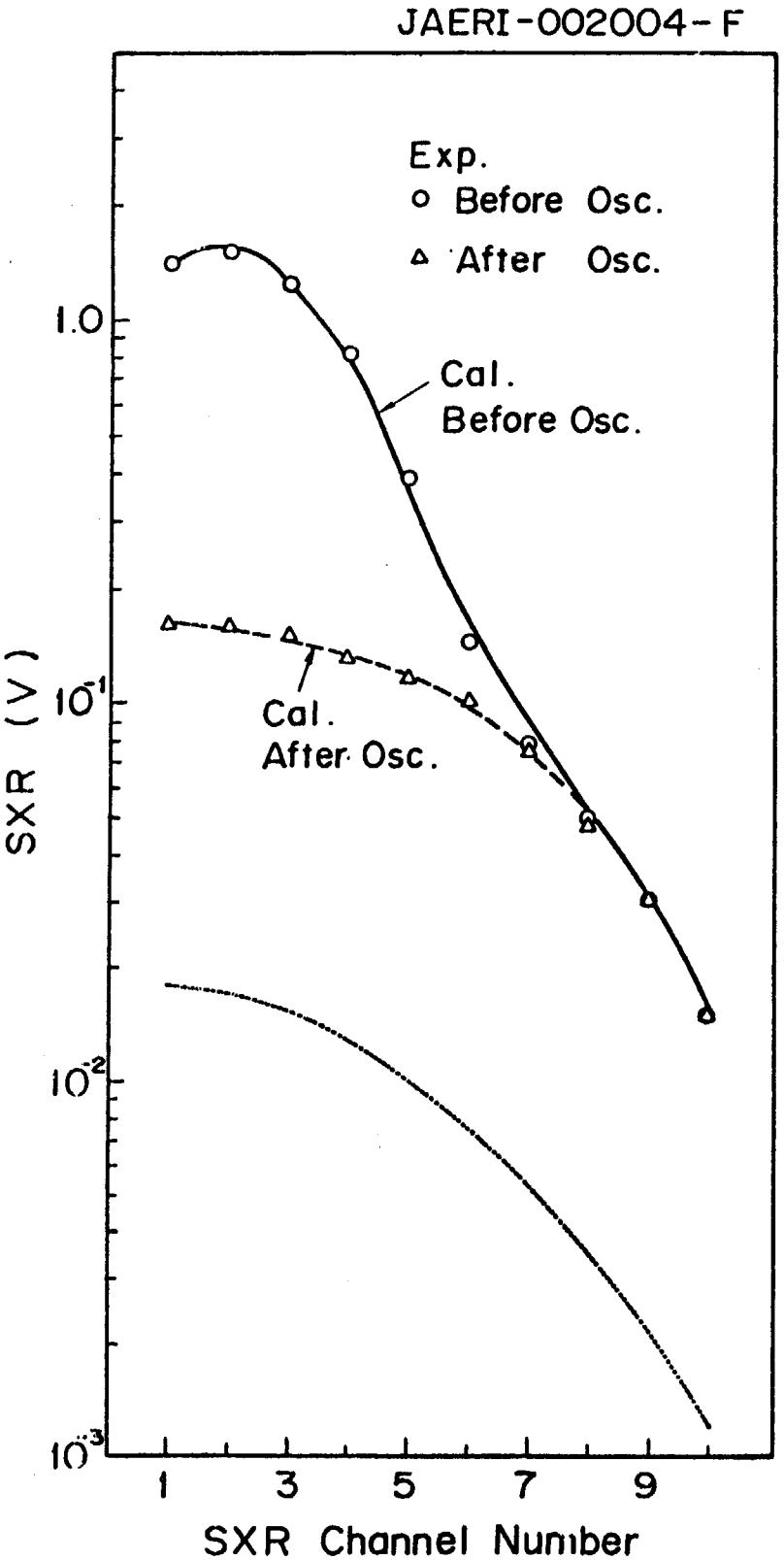

Fig. 4 Profiles of soft X-ray intensity. Marks (O) and (Δ) are observed data before and after MHD activities, respectively. The solid and broken lines are the best fits obtained using the enhancement factors in Fig. 5. The dotted line is hydrogen bremsstrahlung after MHD oscillations assuming a parabolic density profile and using the temperature profile in Fig. 3.

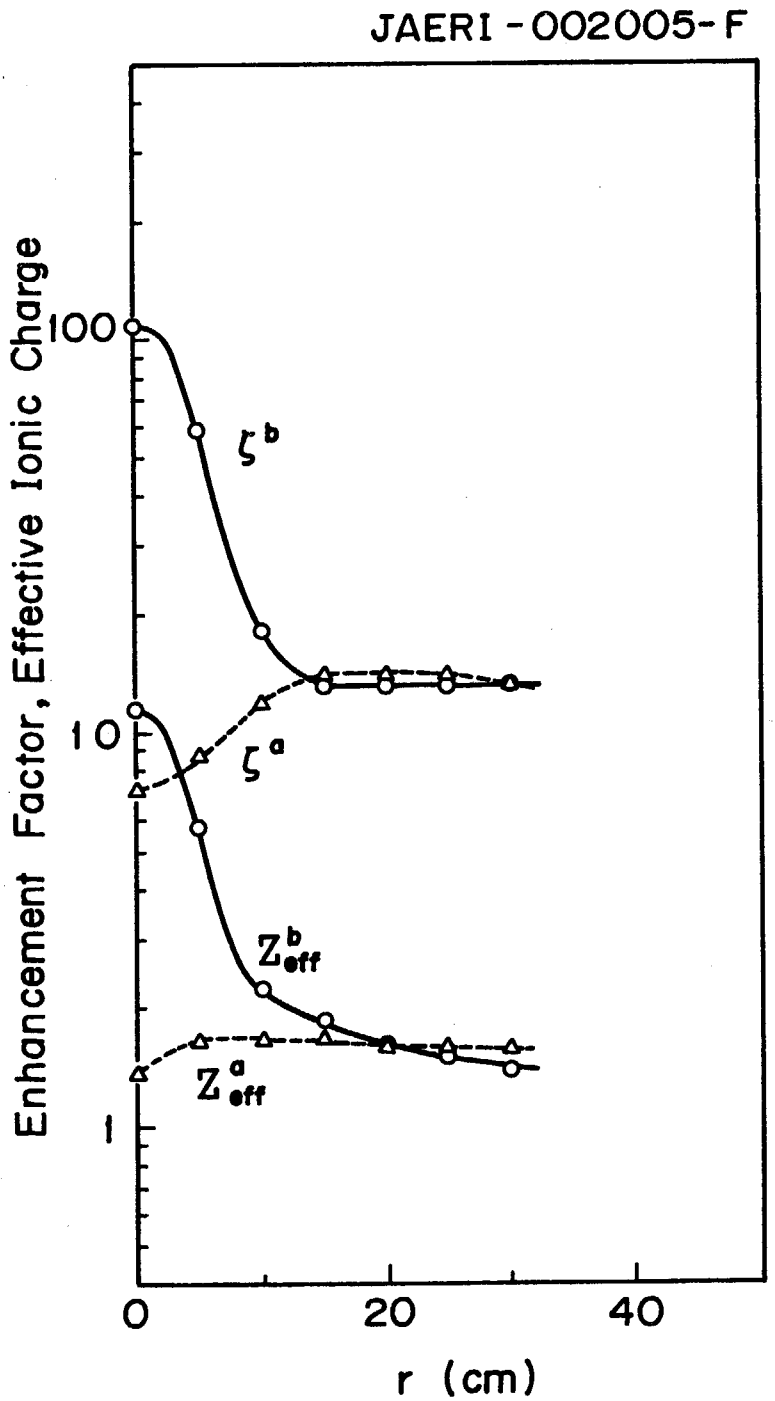

Fig. 5 Radial profiles enhancement factors ζ^b before, and ζ^a after MHD activities giving best fits are shown in Fig. 4.
Profiles of effective ionic charge (Z_{eff}) derived from enhancement factors, assuming that the main impurity is iron.

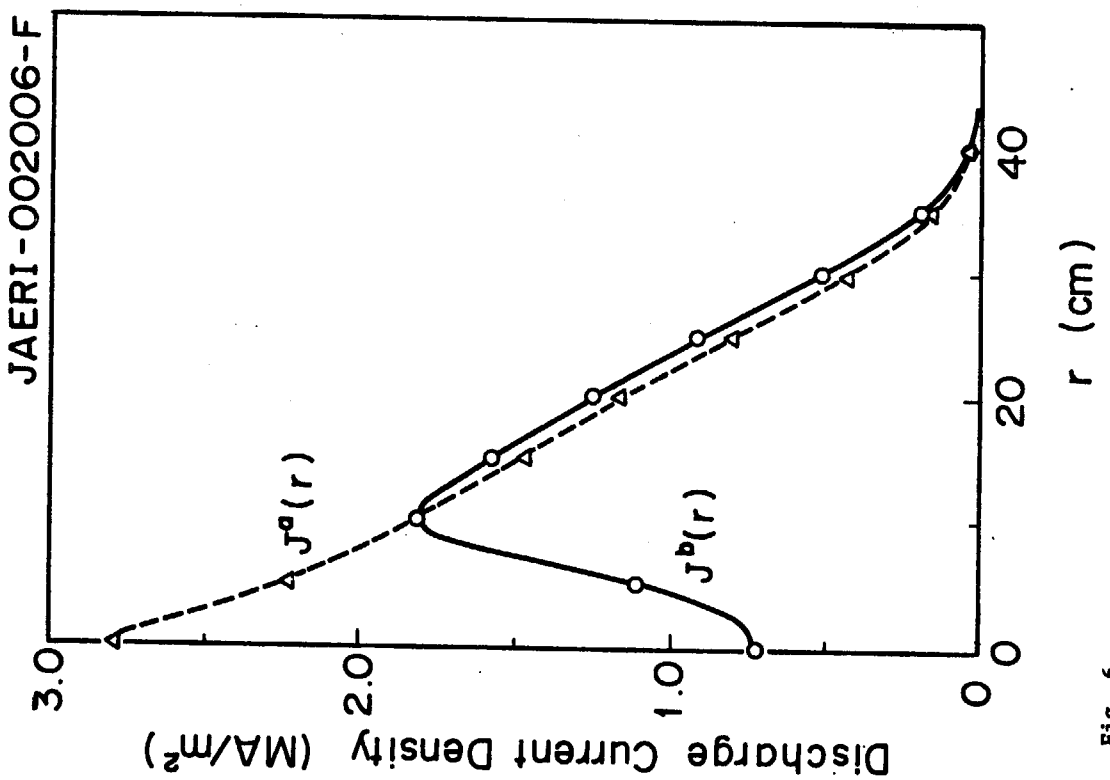

Fig. 6 Radial profiles of discharge current density before and after MHD oscillations calculated from loop voltages, temperature profiles, and effective ionic charge profiles.

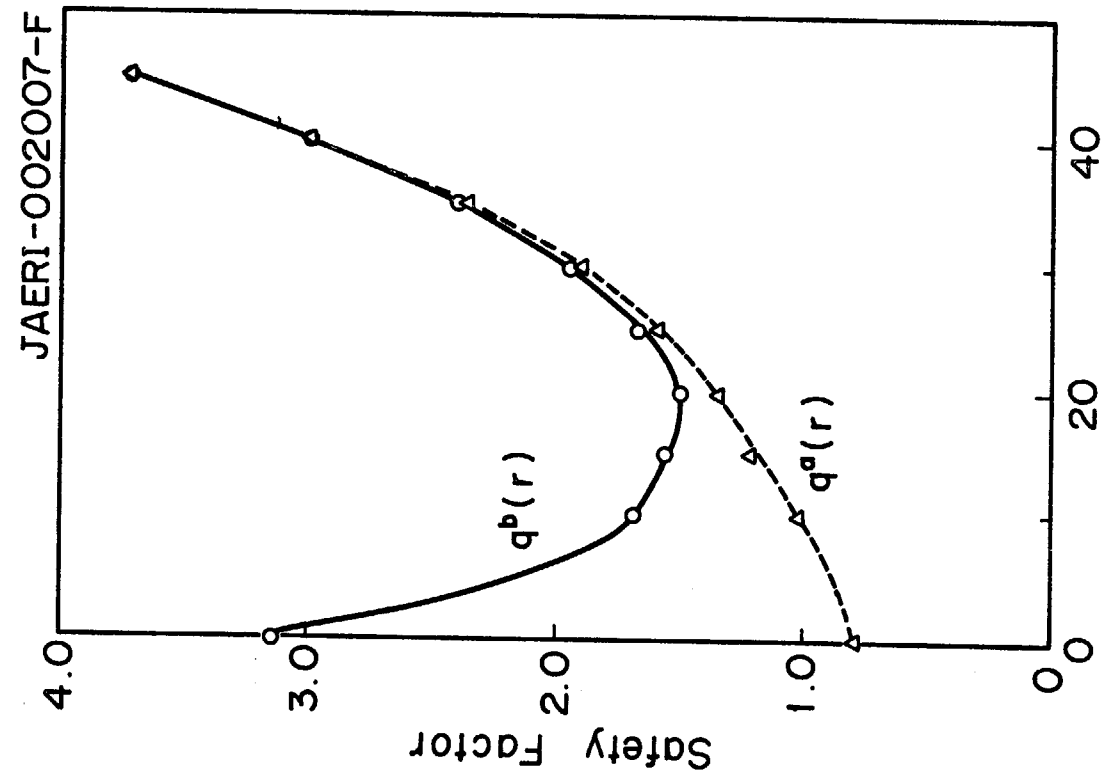

Fig. 7 Profiles of safety factors calculated from profiles of current densities in Fig. 6.